4.1 Curvature Effects (currently listed as 4.4 in the hydraulics book folder; the equations and figure numbers will have to be redone this is indeed changed to 4.4)

Should I use R or R_c instead of ρ for the radius of curvature? Roed's figure must be altered to conform to current notation..

It was noted in Section 2.3 that a semigeostrophic channel flow that has become separated from the left sidewall becomes immune to changes in the position of the right sidewall. As position of the right wall changes the current moves with it, undergoing no other change in cross-sectional form. Only variations in bottom elevation influence the flow in a meaningful way. This aspect has been demonstrated under the usual conditions of gradually varying geometry, implying that the radius of curvature ρ^* of the wall or coastline is large compared to the characteristic width of the current. As we discuss below, the effects of coastal curvature begin to become nontrivial once this restriction is relaxed. In order to make analytical progress, the ratio of the Rossby radius of deformation, though finite, must be kept small. Topographic effects continue to dominate in this limit if the flow contacts the bottom, but topography is irrelevant if the coastal flow takes place in a surface layer, insulated from the bottom by an inactive deeper layer. Sidewall curvature then provides the only forcing mechanism.

Consider a coast-following coordinate system in which s^* and n^* denote the along-shore and offshore directions, as shown in Figure 4.1.1. To motivate the equations of motion in the (n^*,s^*) system, first consider these equations in the more familiar cylindrical (r,θ) system (e.g. Batchelor, 1967, Appendix 2):

$$\frac{\partial u_\theta^*}{\partial t^*} + \frac{u_\theta^*}{r^*}\frac{\partial u_\theta^*}{\partial \theta} + u_r^*\frac{\partial u_\theta^*}{\partial r^*} + \frac{u_r^* u_\theta^*}{r^*} + f u_r^* = -\frac{g}{r^*}\frac{\partial (d^*+h^*)}{\partial \theta}$$

$$\frac{\partial u_r^*}{\partial t} + u_r^*\frac{\partial u_r^*}{\partial r^*} + \frac{u_\theta^*}{r^*}\frac{\partial u_r^*}{\partial \theta} - \frac{u_\theta^{*2}}{r^*} - f u_\theta^* = -g\frac{\partial (d^*+h^*)}{\partial r^*}$$

$$r^*\frac{\partial d^*}{\partial t^*} + \frac{\partial}{\partial \theta}(u_\theta^* d^*) + \frac{\partial}{\partial r^*}\left[r^* u_r^* d^*\right] = 0\,.$$

Here u_r^* and u_θ^* denote the radial and azimuthal velocity and θ increases (and u_θ^* is positive) in the counterclockwise direction. Topographic forcing (terms with h^*) are relevant when the current runs along the bottom and will be retained for completeness. However these will be ignored in our discussion of surface currents.

Now consider a particular location (s^*-value) along the coastline. The radius of curvature $\rho^*(s^*)$ is considered positive if the coast curves to the right in the direction of increasing s. Position the cylindrical coordinates so that the constant-r circles are locally tangent to the coastline at the location in question, as shown in Figure 4.1.1. The origin ($r^*=0$) is positioned a distance $\rho^*(s^*)$ from the coast and therefore $r^*=\rho^*+n^*$ and

$\partial s^* = -\rho^* \partial\theta$. Associating u_r* and -u_θ* with the off-shore and along shore velocity components u* and v* then leads to

$$\frac{\partial v^*}{\partial t^*} + \frac{\rho^*}{\rho^*+n^*} v^* \frac{\partial v^*}{\partial s^*} + u^* \frac{\partial v^*}{\partial n^*} + \frac{u^* v^*}{\rho^*+n^*} - fu^* = -g \frac{\rho^*}{\rho^*+n^*} \frac{\partial (d^*+h^*)}{\partial s^*} \tag{4.1.1}$$

$$\frac{\partial u^*}{\partial t^*} + u^* \frac{\partial u^*}{\partial n^*} + \frac{\rho^*}{\rho^*+n^*} v^* \frac{\partial u^*}{\partial s^*} - \frac{v^{*2}}{\rho^*+n^*} + fv^* = -g \frac{\partial (d^*+h^*)}{\partial n^*} \tag{4.1.2}$$

$$\frac{\rho^*+n^*}{\rho^*} \frac{\partial d^*}{\partial t^*} + \frac{\partial}{\partial s^*}(v^* d^*) + \frac{\partial}{\partial n^*}\left[\frac{\rho^*+n^*}{\rho^*} u^* d^* \right] = 0 \tag{4.1.3}$$

When the coastline curves to the left in the positive s*-direction, so that ρ*<0, the origin of the local cylindrical system lies *offshore* at n*=ρ*. The corresponding singularity appearing in (4.1.1-4.1.3) is avoided if the upper layer outcrops at a value of n*<ρ*, or if the fluid at n*=ρ* is stagnant.

Conservation of potential vorticity in the new coordinates can be expressed as

$$\left[\frac{\partial}{\partial t^*} + u^* \frac{\partial}{\partial n^*} + \frac{\rho^*}{n^*+\rho^*} v^* \frac{\partial}{\partial s^*} \right] q^* = 0 \tag{4.1.4}$$

where

$$q^* = \frac{f + \dfrac{\rho^*}{\rho^*+n^*} \dfrac{\partial u^*}{\partial s^*} - \dfrac{\partial v^*}{\partial n^*} - \dfrac{v^*}{\rho^*+n^*}}{d^*}.$$

Steady flow can be described in terms of a stream function ψ* such that

$$\frac{\partial \psi^*}{\partial n^*} = v^* d^* \qquad \text{and} \qquad \frac{\partial \psi^*}{\partial s^*} = -\frac{\rho^*+n^*}{\rho^*} u^* d^*. \tag{4.1.5}$$

as suggested by (4.1.3). Conservation of the Bernoulli energy and the potential vorticity along streamlines then take the forms:

$$\frac{u^{*2}+v^{*2}}{2} + g(d^*+h^*) = B^*(\psi^*) \tag{4.1.6}$$

and

$$q^*(\psi^*) = \frac{f + \dfrac{\rho^*}{\rho^* + n^*}\dfrac{\partial u^*}{\partial s^*} - \dfrac{\partial v^*}{\partial n^*} - \dfrac{v^*}{\rho^* + n^*}}{d^*} = \frac{f}{D_\infty(\psi^*)}, \qquad (4.1.7)$$

where D_∞ denotes the potential depth.

We will examine a current with width w_e* moving along the coast such that the net transport is in the positive s*-direction. The bottom elevation is constant with n* but may vary with s*. Possible cross sections of the flow are shown in Figures 4.1.2. Let ρ_o* denote the characteristic radius of curvature of the coast, L the scale of s*-variation of the topography, and W the characteristic value of w_e*. Then we can nondimensionalize the above equations using scales (W, L) for (n*,s*) and (V ,U) for (v*,u*), with the latter related by $U=VW/L$. In accordance with usual scaling relations (Section 2.1), $W=(gD)^{1/2}/f$ and $V=(gD)^{1/2}$. The nondimensional forms of (4.1.1-4.1.3) are then

$$\frac{\partial v}{\partial t} + \frac{\rho}{n + \frac{W}{\rho_o^*}\rho} v\frac{\partial v}{\partial s} + u\frac{\partial v}{\partial n} + \frac{W}{\rho_o^*}\frac{uv}{(\rho + \frac{W}{\rho_o^*}n)} - u = -g\frac{\rho}{\rho + \frac{W}{\rho_o^*}n}\frac{\partial(d+h)}{\partial s}, \qquad (4.1.8)$$

$$\frac{W^2}{L^2}\left[\frac{\partial u}{\partial t} + u\frac{\partial u}{\partial n} + \frac{\rho}{\rho + \frac{W}{\rho_o^*}n} v\frac{\partial u}{\partial s}\right] - \frac{W}{\rho_o^*}\frac{v^2}{(\rho + \frac{W}{\rho_o^*}n)} + v = -\frac{\partial(d+h)}{\partial n}, \qquad (4.1.9)$$

and

$$\frac{\rho + \frac{W}{\rho_o^*}n}{\rho}\frac{\partial d}{\partial t} + \frac{\partial}{\partial s}(vd) + \frac{\partial}{\partial n}\left[\frac{\rho + \frac{W}{\rho_o^*}n}{\rho} ud\right] = 0. \qquad (4.1.10)$$

There are two adjustable parameters; the aspect ratios W/L and W/ρ_o*. If the geometry is gradually varying in the sense that W/L<<1, and W/ρ_o* is also <<1, then (4.1.7) will, to leading order, reduce to the geostrophic balance $v = -\partial(d+h)/\partial n$ and all coefficients involving curvature will drop out of the remaining equations. Hence curvature effects disappear from the leading order equations in the limit of small W/L and W/ρ_o*, even though ρ_o* and L might be comparable. This result would appear to be formal justification of the earlier remarks concerning the insensitively of the flow to wall curvature.

There is one exception to the remark just made. If the flow moves near the critical speed (c=0) it becomes sensitive to gradual changes in curvature. As a demonstration, consider the lowest order approximation to (4.1.6-8) when W/L=0, $0<W/\rho_o$*<<1 and when the fluid has uniform potential vorticity. To lowest order the resulting equations are the same as those governing the separated channel flow discussed in Section 2.3. One of the two characteristic forms of these equations is

$$c_- \frac{dR_-}{ds} = O(W / \rho_o^*) \qquad (4.1.11)$$

where c_- is the characteristic speed and R_- is the Riemann invariant [e.g. 2.3.18, 19]. The right-hand side contains the numerically small curvature terms. If c_-=O(1) then dR_-/ds must be O(W/ρ_o^*) implying that the current experiences only slight changes in response to the curvature. On the other hand, a flow that is nearly critical in the sense that $|c_-| = O(W / \rho_o^*)$ will allow dR_-/ds to be $O(1)$ and therefore be sensitive to weak curvature.

One way to include curvature effects in a mathematically simplified setting is to assume $\rho_o^* \approx L$, with $W/L<<1$. Neglecting terms of $O(W/L)^2$ or higher in (4.1.7) leads to an equation in which advection is neglected but centrifugal acceleration is retained. In addition, the local radius of curvature $\rho(s)+n$ is approximated by its value at the coast $\rho(s)$. A common form of the offshore momentum equation that incorporates these approximations is

$$-\frac{v^{*2}}{\rho^*} + fv^* = -g^* \frac{\partial(d^* + h^*)}{\partial n^*}. \qquad (4.1.12)$$

When applied to (4.1.7), the same assumptions lead to

$$\frac{f - \dfrac{v^*}{\rho^*} - \dfrac{\partial v^*}{\partial n^*}}{d^*} = \frac{f}{D_\infty}, \qquad (4.1.13)$$

also valid to O(W^2/L^2). These dimensional forms are unfortunate in that they encourage the belief that centrifugal acceleration v^{*2}/ρ^* can be as large as the Coriolis acceleration fv^*. Equation (4.1.7) clearly shows that W/ρ_o would have to be $O(1)$ in such cases. The operative along-shore length scale L would then be ρ_o and thus $W/L=O(1)$, suggesting that the advective terms in (4.1.7) are no longer negligible. One is then obligated to solve the full shallow-water equations. We will proceed with (4.1.12,13) with the caveat that their validity depends on the curvature terms remaining small compared to the remaining terms.

Most investigations of curvature have assumed that the potential vorticity is uniform (D_∞=*const.*) and that the flow can be traced back into a region where the wall curvature $\kappa=1/\rho$ is zero. In this upstream region the cross-sectional velocity and depth profiles are given by the semigeostrophic solutions (e.g. 2.2.3 and 2.2.4). If the upstream region in question is a reservoir bounded by two sidewalls, the flow is contained in geostrophic boundary currents. If the upstream geometry is coastal, a single boundary current is present.

In a seminal investigation (Röed,1980) considered flow originating from a wide reservoir. Through an unspecified process the reservoir outflow is imagined to separate from the left reservoir wall and become concentrated in a right-wall boundary current of the type shown in Figure 4.1.2a. Given the local value of ρ^* at a particular downstream location, one seeks a solution that preserves the potential vorticity, volume transport, and energy of the reservoir flow. Let gD_r represent the value of the Bernoulli function B^* along the right wall (facing downstream), where the streamfunction ψ^* is taken as zero. Then the relation $dB^*/d\psi^*$ implies $B^*(\psi^*) = gD_r + f\psi^*/D_\infty$. The value of ψ^* along the left wall in the reservoir is Q, the total volume transport, and ψ^* must also take on this value along the free edge $n^* = w_e^*$ of the separated current. The solution at a downstream section where the ρ^* is nonzero may be obtained by first guessing the value w_e^* and then solving the pair of first order ODE's (4.1.12) and (4.1.13), or their dimensional versions, numerically[1]. The integration is started at the free edge $n^* = w_e^*$ of the flow using the conditions $d^*(w_e^*)=0$ and

$$v^*(w_e^*) = \left(2B^*(Q^*)\right)^{1/2} = \left(2(gD_r + fQ^*/D_\infty)\right)^{1/2},$$

which follows from (4.1.6) with $v^{*2} >> u^{*2}$. The integration is then carried to the wall ($n^*=0$), where the condition $\psi^*=0$ is checked. If ψ^* is non-zero at the wall, the value of w_e^* is adjusted and the procedure is repeated until $\psi^*=0$ is obtained at the wall. More than one acceptable value of w_e^* is generally possible.

By implementing this iterative method for various values of ρ^*, one can generate a sequence of cross-sections, all with the same Q^*, D_∞, D_r (and therefore $B^*(\psi^*)$). Figure 4.1.3 contains a dimensionless graph showing solution curves obtained in this way. Each solid curve gives the stream width, represented in terms of $\tanh\left[w_e^* f / 2(gD_\infty)^{1/2}\right]$ as a function of the wall curvature, represented by $\tanh\left[2(gD_\infty)^{1/2}/\rho^* f\right]$. The dimensionless value of the wall energy $\hat{D}_r = D_r(2g/fQ)^{1/2}$ is conserved along each solution curve and [ ]=4 for all curves. Each curve has an upper and lower branch and direct calculation of the speed of the frontal wave that propagates on the free edge indicates that the upper branch is subcritical and the lower branch supercritical.[2] The lower dashed line corresponds to critical flow, as indicated by the merger of subcritical and supercritical solution branches. Just above it lies a second dashed line that marks solutions with zero velocity at the wall. Above this curve the solutions have reverse flow near the wall. This condition, which cannot occur when the flow is subcritical, is closely related the stagnation condition discussed in connection with upstream gyres (Section 2.7). Although the plot extends over the whole range

[1] Röed actually solved these equations with full variable curvature (ρ replaced by $\rho+n$).

[2] Since the curvature is assumed small, the characteristic speeds are approximately given by semigeostrophic theory (see equation 2.3.18).

$-\infty < 2(gD_\infty)^{1/2} / \rho^* f < \infty$ the equations used to derive the solutions are formally valid only for $\left|2(gD_\infty)^{1/2} / \rho^* f\right| << 1$.

The solution curves of Figure 4.1.3 have several notable features. First, the subcritical branches of the curves show that the stream width decreases and approaches a critical state as the curvature decreases. A subcritical current originating upstream along a straight wall ($\rho \to \infty$) will therefore narrow and become less subcritical if the wall bends to the left (facing downstream). The same current becomes wider and more subcritical if the wall bends to the right. If the wall bends to the left and its curvature becomes sufficiently large, the flow will undergo a subcritical-to-supercritical transition at the point of maximum curvature. Downstream the flow will become supercritical and will continue to narrow as the positive curvature decreases. If this supercritical flow then moves into a stretch of negative coastline curvature it can either narrow or widen depending on the particular value of $\hat{D}_r$. Thus, there is no simple rule governing the widening or narrowing of a supercritical current as the coastline curvature varies. The reader will also note that the dependence of the width on curvature is rather weak for many of the solutions curves, at least when $\left|f / 2\rho(gD_\infty)^{1/2}\right| << 1$. This behavior is consistent with the earlier finding that curvature effects are weak in the long wave limit. An exception to this rule occurs when $\hat{D}_r = 2.0$. The corresponding current is exactly critical along the upstream section of strait coastline and will experience a rapid widening or narrowing upon encountering slight finite ρ. This is just an example of the sensitivity of a critical flow to its geometric constraints, anticipated by (4.1.11).

The separation of coastal currents due to coastline curvature is a subtle problem but one of potentially great oceanographic importance. The Gulf Stream, the Kuroshio, and the surface inflow through the Strait of Gibraltar are just three of many examples of boundary flows that experience separation. In the first two cases the separation is from a 'left-hand' boundary and almost certainly involves the variation in f with latitude. The Gibraltar inflow separates from a 'right-hand' boundary (the Moroccan coast) at a sharp corner (Figure 4.1.4) that marks the beginning of the Alboran Sea. The latter contains the anticyclonic Alboran Gyre (Figure 4.1.4). To compare features like this with the (Röed, 1980) model it should first be noted that the model permits two types of separation. In the first, the active layer remains in contact with the wall but a stagnation point forms there. This type of separation is demonstrated in a laboratory experiment (Figure 4.1.5) based on the Strait of Gibraltar and Alboran Sea geometry. In terms of the Röed theory, the value of ρ^* required for separation is indicated by the upper dashed line in Figure 4.1.3, where the flow is slightly subcritical. If the flow is subcritical upstream and supercritical downstream, then the separation streamline will extend from the stagnation point *upstream* into the supercritical flow. To achieve the downstream separation that is characteristic of, say, the Alboran Gyre, the flow would have to be supercritical upstream and subcritical downstream. It is quite possible that the Mediterranean surface inflow leaves the Strait of Gibraltar in a supercritical state, which would permit this scenario.

The second type of separation involves the detachment of the entire upper layer from the coast and the surfacing of the underlying fluid. It may seem surprising that the flow can outcrop on both sides and still maintain a positive flux, but this is made possible by centrifugal acceleration. If (4.1.12) is integrated across the upper layer, the transport can be shown to obey

$$Q = \frac{g' d^{*2}(0)}{2f} + \frac{1}{\rho^*}\int_0^{w_e^*} d^* v^{*2} dn, \qquad (4.1.14)$$

and thus a positive Q may be maintained by a positive ρ^* even when the wall depth $d^*(0)$ vanishes. Some of Roed's solutions undergo this type of separation for sufficiently small ρ^*, but the necessary conditions are not discussed. Klinger (1994) revisited this issue using essentially the same model and found that the radius of curvature required is roughly equal to the inertial radius $\overline{v}_u^*/f$ based on the average velocity of the upstream flow (measured where the wall curvature is zero). There is a tacit assumption concerning the unidirectional nature of the upstream flow here; clearly if the upstream flow is nearly separated, the flow may easily separate for large values of ρ^*. Klinger also explores a configuration in which the lower layer does not have an offshore outcrop (Figure 4.1.2b). Here the moving portion of the current is separated from a stagnant offshore region by a free streamline. The potential vorticity of the flow is again constant but the separation condition is found to be insensitive to its value. Despite the finite offshore depth, the wall depth may again go to zero causing the flow to separate. The separation condition over much of the parameter space of the solution is $\rho^* < 0.9\overline{v}_u^* w_{eu}^*/(g' d_I^*)^{1/2}$, where w_{eu}^* is the upstream current width and d_I^* is the interior depth. If the upstream width w_{eu}^* scales with the deformation radius $(g' d_I^*)^{1/2}/f$ then the criterion is nearly the same as for the first case. Again, this condition may violate the assumption of small wall curvature that underpins the model.

Berry also discusses the case shown in Figure 4.4.2c, where the flow is negative. This corresponds to flow with the wall to the left and is similar to the model of Ou and di Ruijter discussed below. He is able to get his numerical calculations for the critical curvature to collapse along a fairly tight curve (see his Figure 6), but there is absolutely no discussion of a fit to this curve or of a separation law. I need to ask him about this.

A similar technique can be used to explore the case with the wall to the left of positive Q (Figure 4.1.2b). Ou and de Ruijter (1986) use a model that is similar in construct to that considered by Klinger for flow with the wall to the left. The potential vorticity of the moving fluid is constant and the flow is joined to a stagnant offshore region that has lower potential vorticity. The hydraulically relevant wave is now a Kelvin wave that attempts to propagate upstream. Its speed is approximated by $-(g/D_\infty)^{1/2}$ times the wall depth (*cf.* Equation 2.2.26) provided the potential vorticity front lies more than a distance $(gD_\infty)^{1/2}/f$ offshore. Under this condition the flow remains subcritical as long as the wall depth is finite. If d vanishes at the wall, leading to separation of the current, the flow is close to the critical speed. [This property is valid as long as the radius of curvature remains large compared to the current width.] The criticality of the

separated current downstream depends upon the environment in which it propagates; upstream propagation of long waves may or may not be permitted. Curving of the wall to the left of the direction of flow encourages broadening of the boundary current and separation of the flow, whereas negative curvature has the opposite effect. Ou and de Ruijter also takes into account variations in the value of f along the wall and the resulting models is sufficiently complicated that no simple criterion for separation is written down. However, unlike the case of unidirectional flow with the wall on the right, the flow may separate at moderate curvatures.

I am reluctant to include any of Ou and de Ruijter's graphs, as they are quite different from Roed's and include the beta effect.

Laboratory and numerical models allow one to escape the restriction of weak curvature. These studies traditionally seek local criteria for separation as derived from length scales that characterized the flow at a particular location. These include the local radius of curvature, the Rossby Radius of deformation $(g'D)^{1/2} / f$ based on a local upper-layer thickness scale D, and the inertial radius U/f based on the local velocity scale U. The ratio of the last two is a Froude number $F = U / (g'D)^{1/2}$. Many of the experimental flows are set up by a dam break or lock exchange, and this tends to make F close to unity. In such cases the separation criterion is roughly $(g'D)^{1/2} / f\rho \geq 1$ (e.g. Whitehead and Miller, 1979). But since $(g'D)^{1/2} / f$ is roughly equal to U/f the criterion could also have been written as $U/f\rho \geq 1$. One study that allows a range of Froude numbers (Bormans and Garrett, 1989) suggests that the latter is more general. The connection between the experiments and the theory described earlier is difficult to establish, not only because $U/f\rho \geq 1$ violates the underlying assumptions of the models but also because the models stress nonlocal (upstream) separation criteria.

Other complications cloud the picture, suggesting that more than two dimensionless parameters are relevant. Numerical experiments with no-slip boundary conditions produce separation more readily than those with those with free slip conditions. Also, separation is sometimes found to be sensitive to the other factors such as the vorticity distribution in the flow. If the vertical wall is replaced by a sloping bottom or continental shelf the separation condition is altered and the tendencies that occur in response to wall curvature can actually be reversed. (see Section 5.10, to be changed to section 4.??)**.** In the end, flow separation may be sensitive to a whole array of physical circumstances that generic models have difficulty assimilating.

Exercises

1) It was argued in connection with equation (4.1.14) that positive curvature will allow a current of the type shown in Figure 4.1.2a to maintain a positive flux even when depth along the right wall vanishes. Prove that this is also true for a current of the type shown in Figure 4.1.2b.

2) Show that (4.1.12) and (4.1.13) can be solved analytically for the case of zero potential vorticity. Derive the resulting depth and velocity profiles assuming geometry of the form shown in Figure 4.1.2a. For given values of energy gD_r and flux Q what is the condition for separation of the entire upper layer from the right wall. *(Not yet solved: did I assign it as a project?)*

Note that in the case of 'zero potential vorticity' $D_\infty \to \infty$, the curvature terms can be interpreted as augmenting the Coriolis acceleration by an amount $\frac{v}{\rho + n}$.

Figure 4.1.1 Curvalinear coordinate system.

Figure 4.1.2 Upper layer geometry for (a): surface current with the wall to the right of positive flux and an outcropping interface; (b): a similar situation, but with the offshore edge joined to a finite depth, quiescent region by a free streamline; (c) a current running with the wall to the left, facing downstream.

Figure 4.1.3 Solution curves based on Röed,1980. The lower dashed line indicates critical flow and the upper dashed line indicates stagnation along the right wall. The upper branches of the (solid) solution curves correspond to subcritical flow. $\hat{D}_r = D_r(2g / fQ)^{1/2}$ is conserved along each solution curve and [ ]=4 for all curves

Figure 4.1.4 The Alboran Gyre visualized by NOAA/AVHRR *This is a figure downloaded from the web and referenced to Heburn et al. 1990. The right-hand panel is the better of the two. The complete reference only needs to be tracked down if a better image of the Gyre, and particularly the separation of the inflow, can be found.*

Figure 4.1.5 Flow separation in a two-layer lock-exchange flow. The (clear) surface layer enters the gap from the left reservoir and separates from the boundary at the indicated stagnation point. The separated flow continues in an anticyclonic arc, forming a gyre. The denser layer is dyed black and is exposed to the surface offshore (to the right) of the gyre. The experiment is described more fully in Miller and Whitehead, 1979.

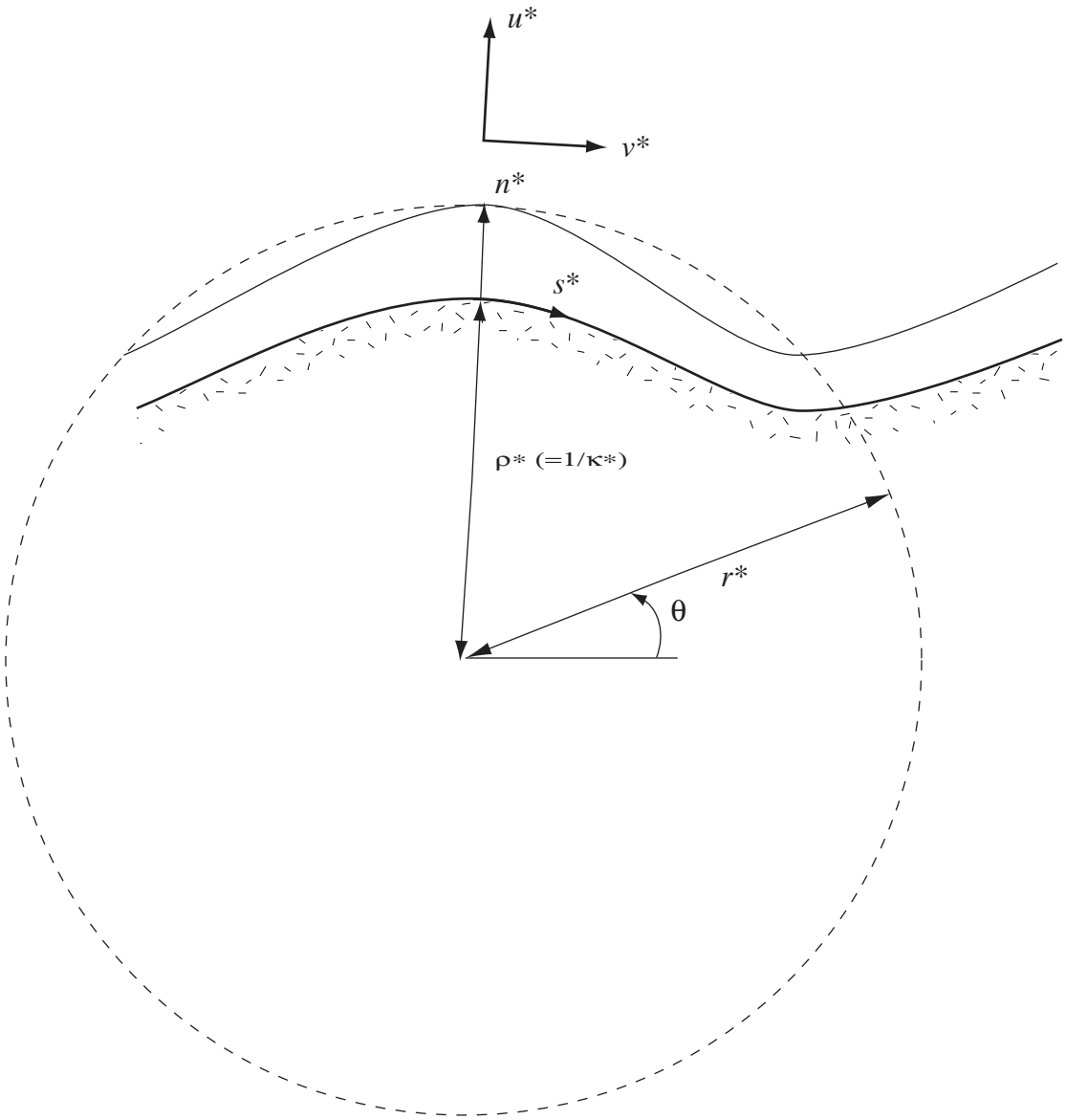

Fig. 4.5.1

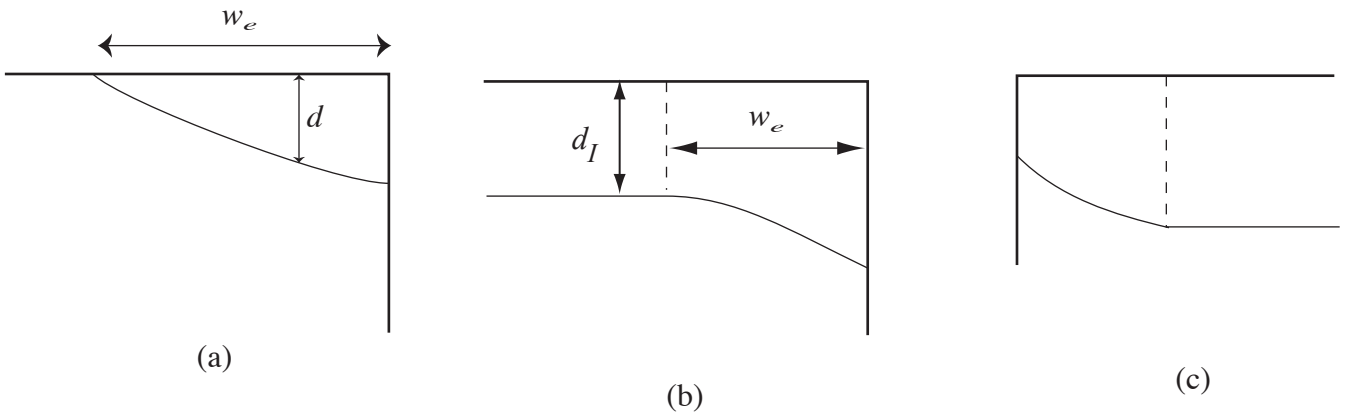

(a) (b) (c)

Fig. 4.5.2

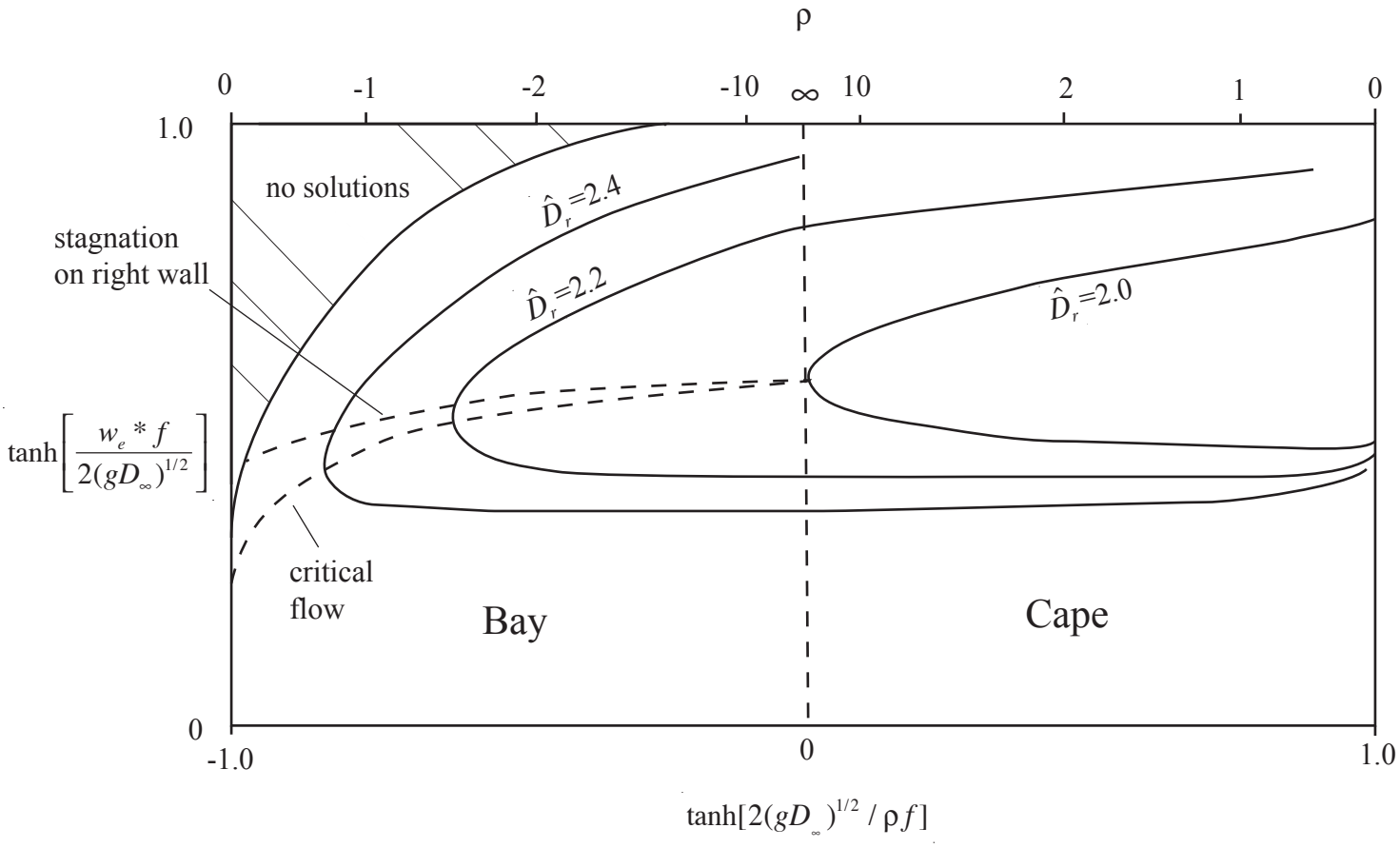
ρ
0
-1
-2
-10
∞
10
2
1
0
1.0
no solutions
stagnation
on right wall
$\hat{D}_r$=2.4
$\hat{D}_r$=2.2
$\hat{D}_r$=2.0
$\tanh\left[\frac{w_e * f}{2(gD_\infty)^{1/2}}\right]$
critical
flow
Bay
Cape
0
-1.0
0
1.0
$\tanh[2(gD_\infty)^{1/2} / \rho f]$

Fig. 4.1.3

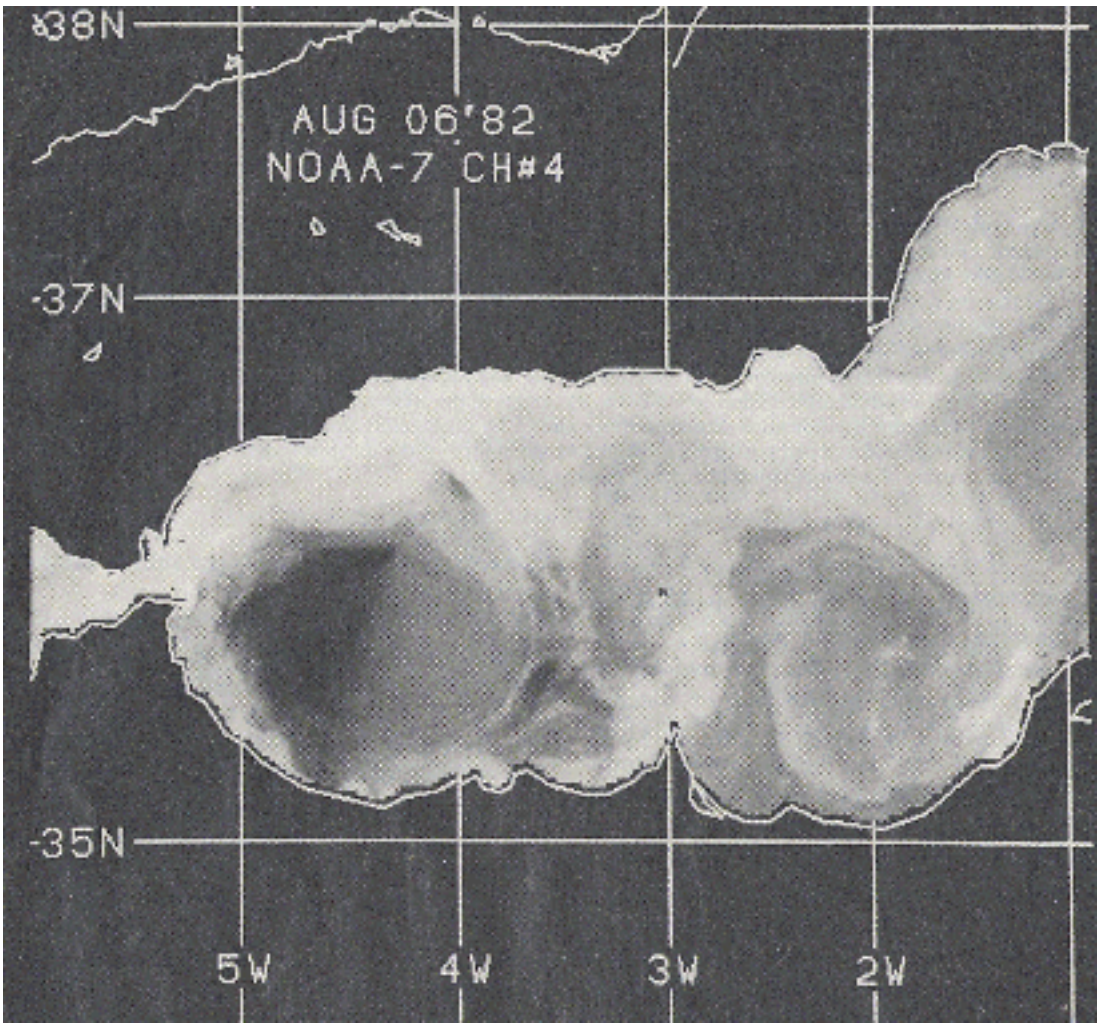
38N
AUG 06'82
NOAA-7 CH#4
37N
35N
5W
4W
3W
2W

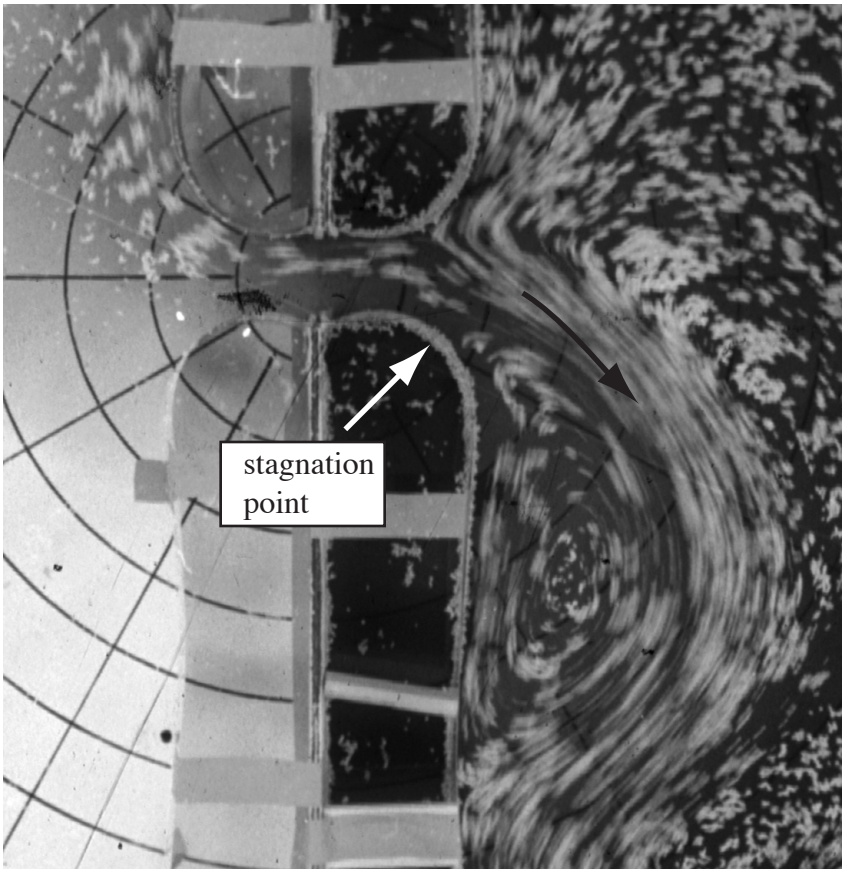

Fig. 4.5.5